PLL with MAF-Based Prefiltering Stage

Small-Signal Modeling and Performance Enhancement

Golestan, Saeed; Guerrero, Josep M.; Vidal, Ana; Yepes, Alejandro G.; Doval-Gandoy, Jesus

Published in:
I E E E Transactions on Power Electronics

DOI (link to publication from Publisher):
10.1109/TPEL.2015.2508882

Publication date:
2016

PLL with MAF-Based Prefiltering Stage: Small-Signal Modeling and Performance Enhancement

Saeed Golestan, *Senior Member, IEEE*, Josep M. Guerrero, *Fellow, IEEE*, Ana Vidal, *Member, IEEE*, Alejandro G. Yepes, *Member, IEEE*, and Jesus Doval-Gandoy, *Member, IEEE*

***Abstract*—In three-phase applications, the synchronous-reference frame phase-locked loop (SRF-PLL) is a standard PLL, which benefits from a simple structure and satisfactory performance under symmetrical and undistorted grid conditions. Under unbalanced and harmonically distorted conditions, however, it suffers from a very poor performance in the detection of grid voltage parameters. To deal with this challenge, incorporating different filters inside its control loop or before its input has been proposed. Recently, using the moving average filter (MAF) as the SRF-PLL prefiltering stage has been suggested in several works. The MAF is a linear-phase filter that can behave like an ideal low-pass filter under certain conditions. The main aim of this letter is to derive the small-signal model of the SRF-PLL with MAF-based prefiltering stage (briefly called the PMAF-PLL), which has not been presented before. This model enables the designer to simply analyze the stability condition and dynamic behavior of the PMAF-PLL. After developing the model, a simple modification to enhance the PMAF-PLL performance under frequency varying environments is presented. Finally, the equivalence of PMAF-PLL and the space-vector Fourier Transform based PLL (SVFT-PLL), which is a well-known PLL in three-phase applications, is proved. This equivalence implies that the small-signal model of the PMAF-PLL and the method presented to enhance its performance are valid for the SVFT-PLL.**

***Index Terms*—Moving average filter (MAF), phase-locked loop (PLL), synchronization.**

I. Introduction

Besides the problem of grid voltage imbalance, which may be due to asymmetrical voltage sags, single-phase loading and grid impedance imbalance, the synchronization of grid-connected power electronics based equipment is facing more serious challenges: presence of dc offset and large harmonic components in the grid voltage; while the former may be caused by grid faults, A/D conversion, measurement devices, etc. [1], the latter is commonly due to the proliferation of power electronics based nonlinear loads [2]. To deal with these challenges, many advanced synchronization techniques have been developed in recent years. Most of these techniques are based on phase-locked loops (PLLs) [3].

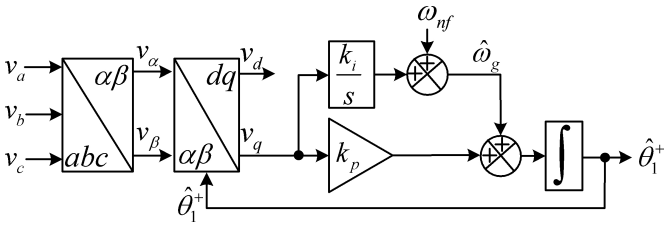

Fig. 1. Schematic diagram of the SRF-PLL.

Fig. 1 shows the schematic diagram of the standard synchronous-reference frame PLL (SRF-PLL), which is a standard PLL in three-phase applications. In the SRF-PLL, the three-phase voltages are transformed into the *dq* reference frame by applying the Clarke's transformation and then the Park's transformation. The signal v_q (or v_d, depending on the Park's transformation), which contains the phase error information, is then fed to a proportional-integral (PI) controller to ensure a zero average phase error under both phase-angle jumps and frequency drifts. The SRF-PLL has a limited disturbance (dc offset, harmonic, and imbalance) rejection capability. To deal with this issue, including additional filter(s) either inside the SRF-PLL control loop or before its input has been proposed. The conventional infinite impulse response low-pass filters [4], the moving average filter (MAF) [5]-[7], the notch filter [8], the *dq*-frame delayed signal cancellation operator [9]-[11] and the repetitive regulator [12] are well-known in-loop filtering techniques, and the complex coefficient filters [13], [14], the recursive discrete Fourier transform [15], the $\alpha\beta$-frame delayed signal cancellation operator [10]-[11], [16]-[17], and the dual second-order generalized integrators [18] are popular prefiltering techniques.

Recently, using the MAF as the SRF-PLL prefiltering stage has been proposed in several works [19]-[21]. The schematic diagram of the SRF-PLL with MAF-based prefiltering stage (hereafter, briefly called the PMAF-PLL) can be observed in Fig. 2. In the PMAF-PLL, the SRF-PLL and MAF-based prefiltering stage are both working in the synchronous-reference frame, but with different rotating angles. This rotating angle difference has made the small-signal modeling and, consequently, the stability and dynamic behavior analysis of the

This work was supported in part by the Research Programme on Microgrids, Department of Energy Technology, Aalborg university, and in part by the Spanish Ministry of Science and Innovation and by the European Commission, European Regional Development Fund (ERDF) under project DPI2012-31283.

S. Golestan, and J. M. Guerrero are with the Department of Energy Technology, Aalborg University, Aalborg DK-9220, Denmark (e-mail: s.golestan@ieee.org; joz@et.aau.dk).

A. Vidal, A G. Yepes, and J. Doval-Gandoy are with the Department of Electronics Technology, University of Vigo, Vigo 36310, Spain (e-mail: anavidal@uvigo.es; agyepes@uvigo.es; jdoval@uvigo.es).

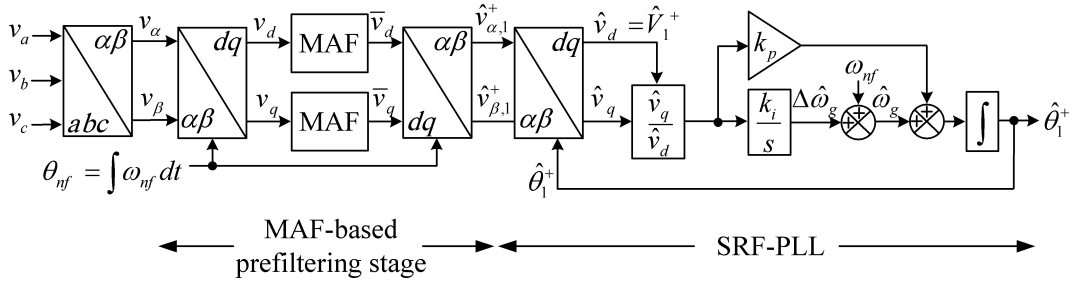

Fig. 2. Schematic of the SRF-PLL with MAF-based prefiltering stage (PMAF-PLL).

PMAF-PLL difficult. The main aim of this letter is to derive an accurate small-signal model for the PMAF-PLL, which to the best of the authors' knowledge, has not been presented before. The performance enhancement of the PMAF-PLL in the presence of frequency drifts is another objective of this letter. Finally, the equivalence of PMAF-PLL and space-vector Fourier Transform based PLL (SVFT-PLL) [22], [23], which is a well-known PLL in three-phase applications, is proved. This equivalence implies that the small-signal model of the PMAF-PLL and the method presented to enhance its performance are valid for the SVFT-PLL.

II. Moving Average Filter

The MAF is a linear-phase filter, which is defined in the continuous-time and discrete-time domains as

$$\bar{v}(t) = \frac{1}{T_w}\int_{t-T_w}^{t} v(\tau)\, d\tau \tag{1}$$

$$\bar{v}(k) = \frac{1}{N}\sum_{n=0}^{N-1} v(k-n) \tag{2}$$

where v and $\bar{v}$ are the input and output signals of the MAF, respectively, $T_w = NT_s$ is the MAF window length, N is the number of samples within the window length, and T_s is the sampling time.

The s-domain and z-domain transfer functions of the MAF can be simply obtained using (1) and (2) as

$$G_{MAF}(s) = \frac{\bar{v}(s)}{v(s)} = \frac{1-e^{-T_w s}}{T_w s} \tag{3}$$

$$G_{MAF}(z) = \frac{\bar{v}(z)}{v(z)} = \frac{1}{N}\sum_{n=0}^{N-1} z^{-n} = \frac{1}{N}\frac{1-z^{-N}}{1-z^{-1}}. \tag{4}$$

Using (3) and (4), the magnitude and phase frequency response of the MAF can be described as

$$G_{MAF}(j\omega) = \left|\frac{\sin(\omega T_w/2)}{(\omega T_w/2)}\right| \angle -\omega T_w/2 \tag{5}$$

$$G_{MAF}\left(e^{j\omega T_s}\right) = \left|\frac{\sin(\omega N T_s/2)}{N\sin(\omega T_s/2)}\right| \angle -\omega(N-1)T_s/2. \tag{6}$$

Notice that (6) converges to (5) if $T_s \to 0$.

It is easy to show using (5) [or (6)] that the MAF has zero gain at frequencies that are integer multiples of $1/T_w$ in Hertz, which means it can completely block the disturbance components at these frequencies. This fact can be clearly observed in Fig. 3, which shows the Bode plot of the MAF for $T_w = T = 0.02$ s and $T_w = T/2 = 0.01$ s (T is the grid nominal period). Throughout this paper, $T_w = 0.02$ s is considered, as this value enables the MAF to completely reject the dc offset and filter out (or at least significantly attenuate) all harmonics before the SRF-PLL input.

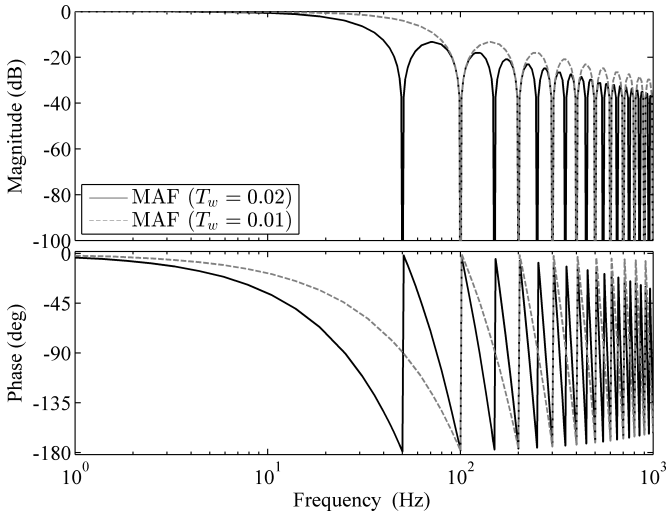

Fig. 3. Bode plot of the MAF for $T_w = 0.02$ s (solid line) and $T_w = 0.01$ s (dashed line) and $T_s = 1e-4$ s.

III. Small-Signal Modeling

As mentioned before, the MAF-based prefiltering stage completely rejects (or at least significantly attenuates) disturbance components before the SRF-PLL input. Thus, the presence of these disturbances are neglected during the modeling procedure and the three-phase input voltage of the PMAF-PLL is considered to be in the discrete-time domain as

$$\begin{aligned} v_a(k) &= V_1^+ \cos\left(\theta_1^+(k)\right) \\ v_b(k) &= V_1^+ \cos\left(\theta_1^+(k) - 2\pi/3\right) \\ v_c(k) &= V_1^+ \cos\left(\theta_1^+(k) + 2\pi/3\right) \end{aligned} \tag{7}$$

where V_1^+ and θ_1^+ are the amplitude and angle of the grid voltage fundamental component, respectively.

Applying the Clarke's transformation and then the Park's transformation with a rotating angle θ_n to the three-phase

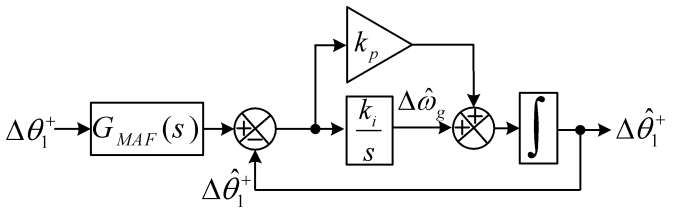

Fig. 4. Small-signal model of the PMAF-PLL in the s-domain.

voltages (7) gives the MAFs input signals as

$$\begin{aligned} v_d(k) &= V_1^+ \cos\overbrace{\left(\theta_1^+(k) - \theta_n(k)\right)}^{\Delta\theta_1^+(k)} \\ v_q(k) &= V_1^+ \sin\left(\theta_1^+(k) - \theta_n(k)\right). \end{aligned} \tag{8}$$

Considering the discrete time definition of the MAF, i.e., (2), the MAF output signals can be expressed as

$$\begin{aligned} \bar{v}_d(k) &= \tfrac{1}{N}\sum_{n=0}^{N-1} v_d(k-n) = \tfrac{V_1^+}{N}\sum_{n=0}^{N-1}\cos\left(\Delta\theta_1^+(k-n)\right) \\ \bar{v}_q(k) &= \tfrac{1}{N}\sum_{n=0}^{N-1} v_q(k-n) = \tfrac{V_1^+}{N}\sum_{n=0}^{N-1}\sin\left(\Delta\theta_1^+(k-n)\right). \end{aligned} \tag{9}$$

Applying the inverse Park's transformation with rotating angle θ_n and subsequently the Park's transformation with rotating angle $\hat{\theta}_1^+$ to the output signals of the MAFs gives

$$\hat{v}_q(k) = \frac{V_1^+}{N}\sum_{n=0}^{N-1}\sin\left(\Delta\theta_1^+(k-n) - \Delta\hat{\theta}_1^+(k)\right) \tag{10}$$

where $\Delta\hat{\theta}_1^+ = \hat{\theta}_1^+ - \theta_n$. By approximating the sine functions with their arguments, (10) can be rewritten by

$$\begin{aligned} \hat{v}_q(k) &\approx \frac{V_1^+}{N}\sum_{n=0}^{N-1}\left(\Delta\theta_1^+(k-n) - \Delta\hat{\theta}_1^+(k)\right) \\ &= \left[\frac{V_1^+}{N}\sum_{n=0}^{N-1}\Delta\theta_1^+(k-n)\right] - V_1^+\Delta\hat{\theta}_1^+(k). \end{aligned} \tag{11}$$

Taking the z-transform from both sides of (11) yields

$$\hat{v}_q(z) \approx V_1^+\left(G_{MAF}(z)\Delta\theta_1^+(z) - \Delta\hat{\theta}_1^+(z)\right) \tag{12}$$

which corresponds in the s-domain to

$$\hat{v}_q(s) \approx V_1^+\left(G_{MAF}(s)\Delta\theta_1^+(s) - \Delta\hat{\theta}_1^+(s)\right). \tag{13}$$

Using (13) and Fig. 2, the small-signal model of the PMAF-PLL in the s-domain can be obtained as shown in Fig. 4. Notice that the grid voltage amplitude V_1^+ does not appear in the model because there is an amplitude normalization right before the PI controller.

To evaluate the accuracy of the derived model, the actual PMAF-PLL and its model are simulated in the Matlab/Simulink environment and their results under a phase-angle jump and a frequency step change are obtained and compared to each other. For both the PMAF-PLL and the small-signal model, the control parameters are considered to be $k_p = 400$, $k_i = 40000$, $T_w = 0.02$ s, $T_s = 1e-4$ s, and $V_1^+ = 1$ pu. Fig. 5 illustrates the obtained results. It can be observed that the derived model perfectly predicts the PMAF-PLL dynamic behavior.

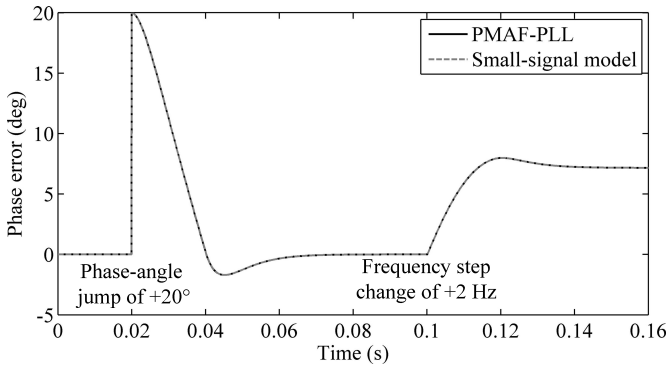

Fig. 5. Accuracy assessment of the PMAF-PLL small-signal model. Parameters: $k_p = 400$, $k_i = 40000$, $T_w = 0.02$ s, $T_s = 1e-4$ s, $V_1^+ = 1$ pu, and $\omega_{nf} = 2\pi 50$ rad/s. Before the frequency step change, the grid frequency is at its nominal value, i.e., 50 Hz.

IV. Performance Enhancement Under Frequency-Varying Grid Condition

As Fig. 5 shows, the PMAF-PLL suffers from a phase offset error in the presence of frequency drifts. The reason is that, under off-nominal frequencies, the fundamental component of the grid voltage appears as a component of the frequency $\Delta\omega_g = \omega_g - \omega_{nf}$ in the MAF input, where ω_g is the actual grid frequency and ω_{nf} is the nominal value of the grid frequency. This component experiences a phase-shift equal to

$$\angle G_{MAF}(z = e^{j\Delta\omega_g T_s}) = -\underbrace{0.5\left(T_w - T_s\right)}_{k_\varphi}\Delta\omega_g \tag{14}$$

when passing through the MAF. As a result, the phase of the fundamental component extracted by the PMAF-PLL prefiltering stage will be $\theta_1^+ - k_\varphi\Delta\omega_g$ in the steady state. Neglecting the nonlinearity caused by the SRF-PLL phase detector and amplitude normalization stage, the input signal of the PI controller can be well approximated by $(\theta_1^+ - k_\varphi\Delta\omega_g) - \hat{\theta}_1^+$, which is the difference of the phase-angle of the SRF-PLL input signal and the rotating angle of its Park's transformation. This phase difference converges to zero in the steady state thanks to the action of the PI controller. As a result, the phase estimated by the SRF-PLL in the steady state will be $\hat{\theta}_1^+ = \theta_1^+ - k_\varphi\Delta\omega_g$, which means the PMAF-PLL suffers from a phase offset error equal to $k_\varphi\Delta\omega_g$. The same conclusion can be drawn using the derived small-signal model.

To deal with this problem, it is suggested in [19]-[21] to incorporate a secondary frequency detector in the prefiltering stage of the PMAF-PLL and use the frequency estimated by it to make the prefiltering stage frequency adaptive. This approach, however, increases the implementation complexity. In what follows, a more straightforward yet effective solution is presented.

The suggested approach in this letter is changing the rotating angle of the Park's transformation of the SRF-PLL to $\hat{\theta}_1^+ - k_\varphi\Delta\hat{\omega}_g$, as highlighted in Fig. 6. This modification changes the PI controller input signal (which, as mentioned before, can

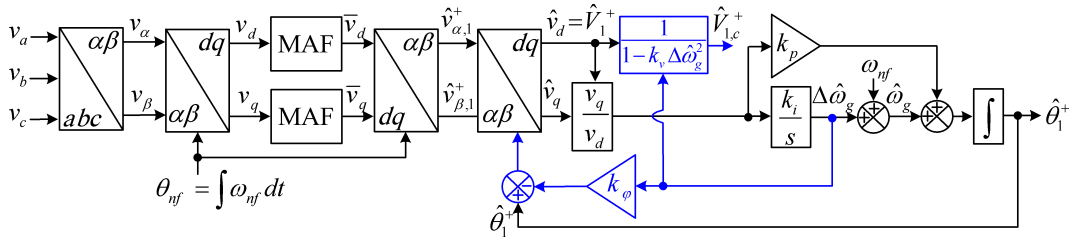

Fig. 6. Schematic of the enhanced PMAF-PLL.

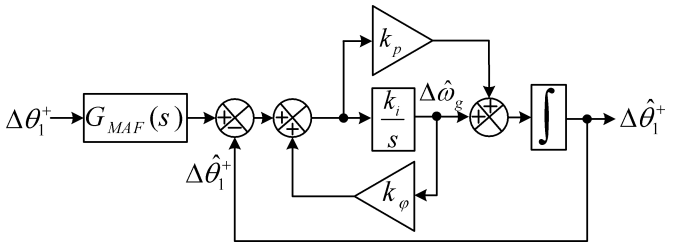

Fig. 7. Small-signal model of the enhanced PMAF-PLL.

be well approximated by the difference of the phase-angle of the SRF-PLL input signal and the rotating angle of the Park's transformation) to $(\theta_1^+ - k_\varphi \Delta\omega_g) - (\hat{\theta}_1^+ - k_\varphi \Delta\hat{\omega}_g)$. Hence, in the steady state, in which the PI controller input signal becomes zero, $\hat{\theta}_1^+ = \theta_1^+$ is achieved.

In a similar manner, it can be shown that there is a small steady-state error in the amplitude estimated by the PMAF-PLL under off-nominal frequencies, as highlighted in (15).

$$\hat{V}_1^+ = \left|G_{MAF}\left(z = e^{j\Delta\omega_g T_s}\right)\right| V_1^+ \approx \underbrace{\left(1 - \frac{T_w^2}{24}\Delta\omega_g^2\right)}_{\text{amplitude error factor}} V_1^+ \tag{15}$$

This error can be corrected by the online calculation of the amplitude error factor using $\Delta\hat{\omega}_g$ and dividing the estimated amplitude $\hat{V}_1^+$ by that, as highlighted in Fig. 6 where $k_v = T_w^2/24$. For the sake of brevity, the structure shown in Fig. 6 is referred to as the enhanced PMAF-PLL.

Fig. 7 shows the small-signal model of the enhanced PMAF-PLL, which can be obtained by following the same procedure used for deriving the PMAF-PLL small-signal model. The accuracy of this model is evaluated under the same tests as in Fig. 5, i.e., under a phase-angle jump of 20° and subsequently a frequency step change of +2 Hz. The obtained results are shown in Fig. 8. The accuracy of the enhanced PMAF-PLL small-signal model and the effectiveness of the suggested approach to eliminate the phase offset error under off-nominal grid frequencies are evident from this figure.

V. Stability Analysis and Parameters Selection

Using Fig. 7, the closed-loop transfer function of the enhanced PMAF-PLL can be obtained as

$$G_{cl}(s) = \frac{\Delta\hat{\theta}_1^+(s)}{\Delta\theta_1^+(s)} = G_{MAF}(s)\frac{k_p s + k_i}{s^2 + \underbrace{(k_p - k_i k_\varphi)}_{2\zeta\omega_n} s + \underbrace{k_i}_{\omega_n^2}} \tag{16}$$

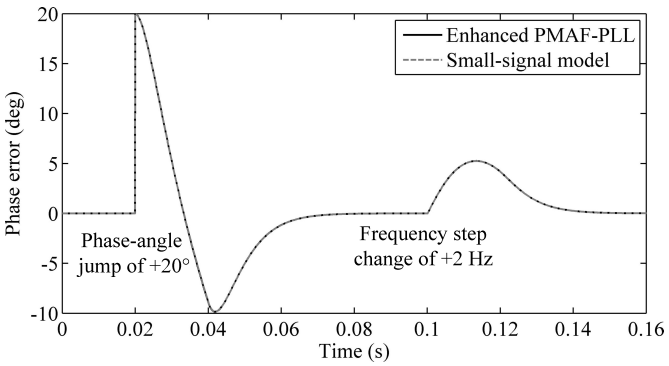

Fig. 8. Accuracy assessment of the enhanced PMAF-PLL small-signal model. Parameters: $k_p = 804$, $k_i = 40426$, $T_w = 0.02$ s, $T_s = 1e-4$ s, $V_1^+ = 1$ pu, and $\omega_{nf} = 2\pi 50$ rad/s.

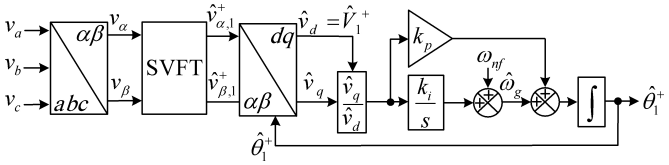

Fig. 9. Schematic of the SVFT-PLL.

where ζ and ω_n denote the damping factor and the natural frequency, respectively. Applying the Routh-Hurwitz's stability test to the PLL characteristic polynomial, i.e., the denominator of (16), gives the stability condition as

$$0 < k_i k_\varphi < k_p. \tag{17}$$

The proportional and integral gains k_p and k_i can be determined by selecting appropriate values for ζ and ω_n. This selection involves tradeoffs between speed of response, overshoot, stability margin, and filtering capability, which has been well discussed in countless publications [11], [24], [25]. Here, $\zeta = 1$ and $\omega_n = 2\pi 32$ rad/s are chosen, which results in $k_p = 804$ and $k_i = 40426$.

VI. Equivalence of PMAF-PLL and SVFT-PLL

The SVFT-PLL [22], [23], as shown in Fig. 9, has a similar structure to the PMAF-PLL (see Fig. 2), but it uses the SVFT instead of MAF-based prefiltering stage for the extraction of the fundamental component of the grid voltage. The z-domain transfer function of the nonrecursive SVFT can be expressed as

$$G_{SVFT}(z) = \frac{1}{N}\sum_{n=0}^{N-1} e^{\frac{j2\pi n}{N}} z^{-n}. \tag{18}$$

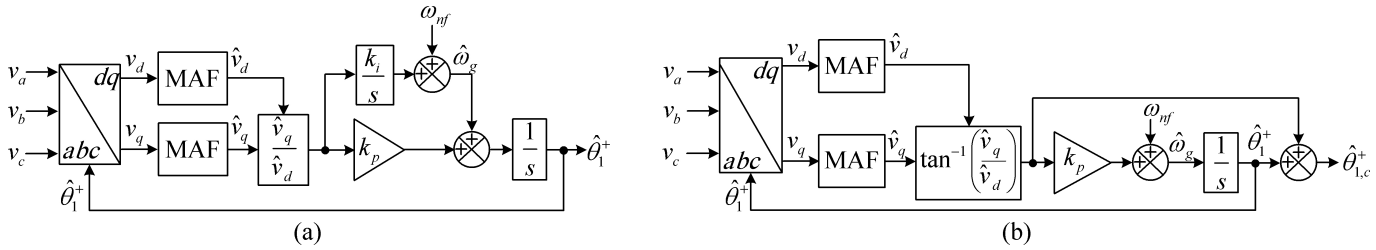

Fig. 10. Schematic of (a) the MAF-PLL and (b) the QT1-PLL.

TABLE I
CONTROL PARAMETERS

	Enhanced PMAF-PLL	Standard MAF-PLL	QT1-PLL
Proportional gain, k_p	804	41.42	49.8
Integral gain, k_i	40426	710.68	—
MAF window length, T_w	0.02 s	0.02 s	0.02 s

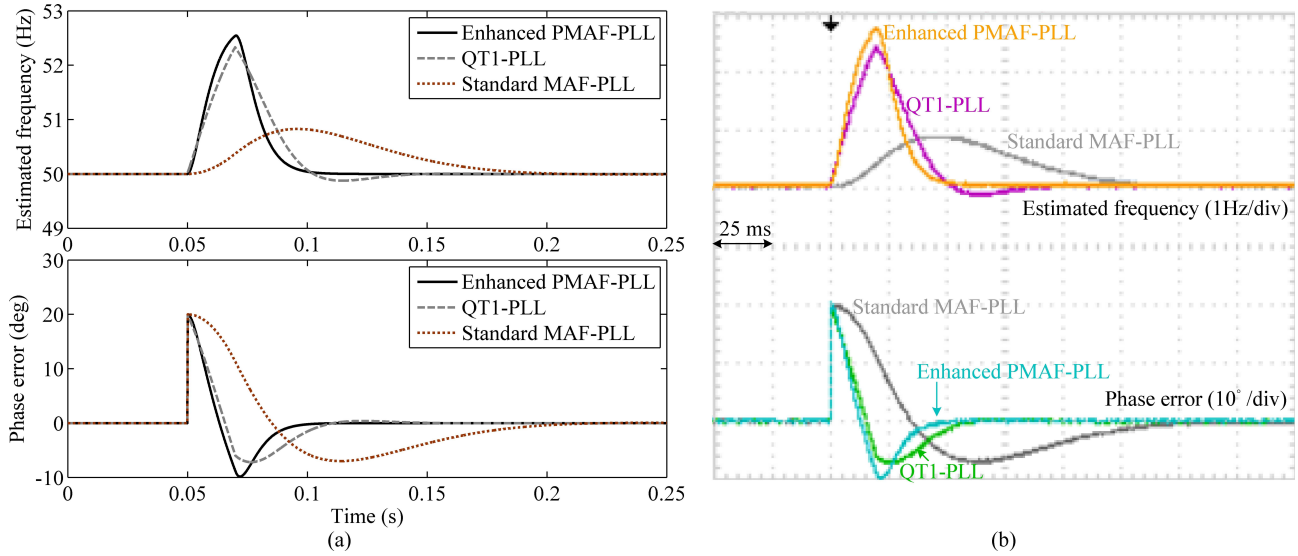

Fig. 11. (a) Simulation and (b) experimental results under the test case 1.

Notice that the SVFT and discrete Fourier Transform (DFT) have the same z-transforms, because the SVFT corresponds to the application of the DFT to a complex signal.

In the space-vector notation, the input-output relation of the MAF-based prefiltering stage in Fig. 2 can be described as

$$\vec{\hat{v}}^{+}_{\alpha\beta,1}(t) = e^{j\theta_{nf}}\left[G_{MAF}(t) * \left(e^{-j\theta_{nf}} v_{\alpha\beta}(t)\right)\right] \tag{19}$$

where $\vec{\hat{v}}^{+}_{\alpha\beta,1}(t) = \hat{v}^{+}_{\alpha,1}(t) + j\hat{v}^{+}_{\beta,1}(t)$, $\vec{v}_{\alpha\beta}(t) = v_\alpha(t) + jv_\beta(t)$, and $*$ denotes the convolution product. Taking the Laplace transform of both sides of (19) yields

$$\frac{\vec{\hat{v}}^{+}_{\alpha\beta,1}(s)}{v_{\alpha\beta}(s)} = G_{MAF}(s - j\omega_{nf}) \tag{20}$$

which corresponds in the z-domain to

$$\frac{\vec{\hat{v}}^{+}_{\alpha\beta,1}(z)}{v_{\alpha\beta}(z)} = G_{MAF}(ze^{-j\omega_{nf}T_s}) = \frac{1}{N}\sum_{n=0}^{N-1} e^{\frac{j2\pi n}{N}} z^{-n}. \tag{21}$$

It can be observed that (18) and (21) are identical, which proves the equivalence of SVFT and MAF-based prefiltering stages. Thanks to this equivalence, it can be concluded that the PMAF-PLL and SVFT-PLL are mathematically equivalent, and therefore, the same small-signal model and properties as those of the PMAF-PLL can be considered for the SVFT-PLL.

VII. SIMULATION AND EXPERIMENTAL RESULTS

In this section, the performance of the enhanced PMAF-PLL is evaluated using simulation and experimental studies. In obtaining all results, the sampling frequency is fixed at 10 kHz. To provide a base for comparison, the standard MAF-PLL [5] and the quasi-type-1 PLL (QT1-PLL) [26] are also implemented and their results are compared with those of the enhanced PMAF-PLL. The schematic of these two PLLs can be observed in Fig. 10. Designing the control parameters of the standard MAF-PLL is carried out using the symmetrical optimum method, as explained in [5]. For the case of the QT1-PLL, the parameter design procedure is more straightforward as the PI controller is replaced with a simple gain. This gain is selected so that the minimum 2% settling time in response to

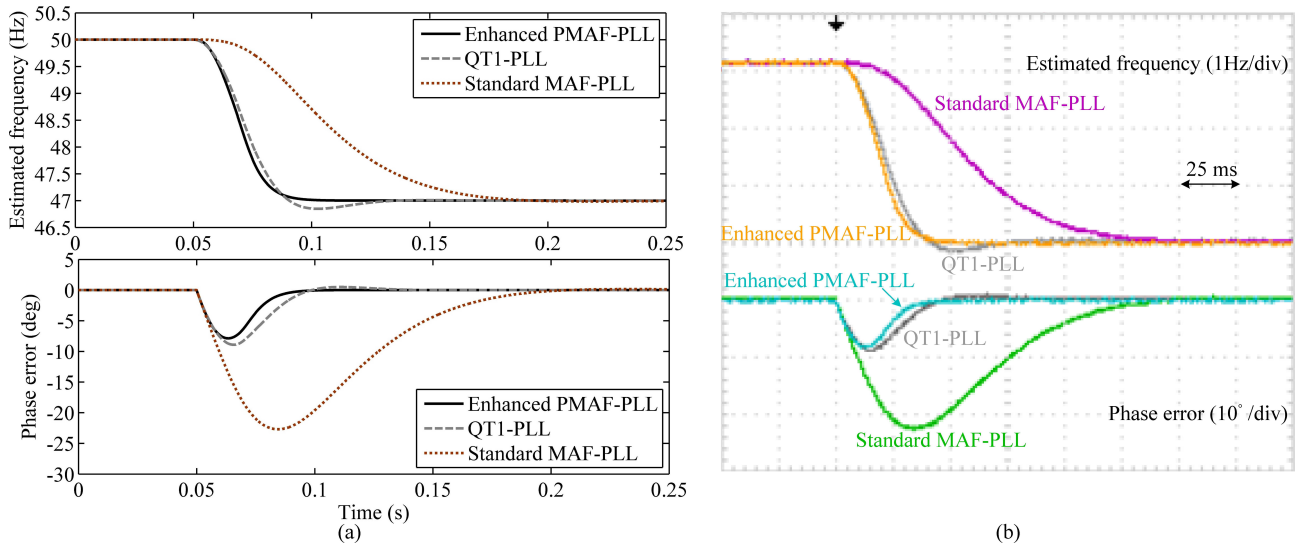

Fig. 12. (a) Simulation and (b) experimental results under the test case 2.

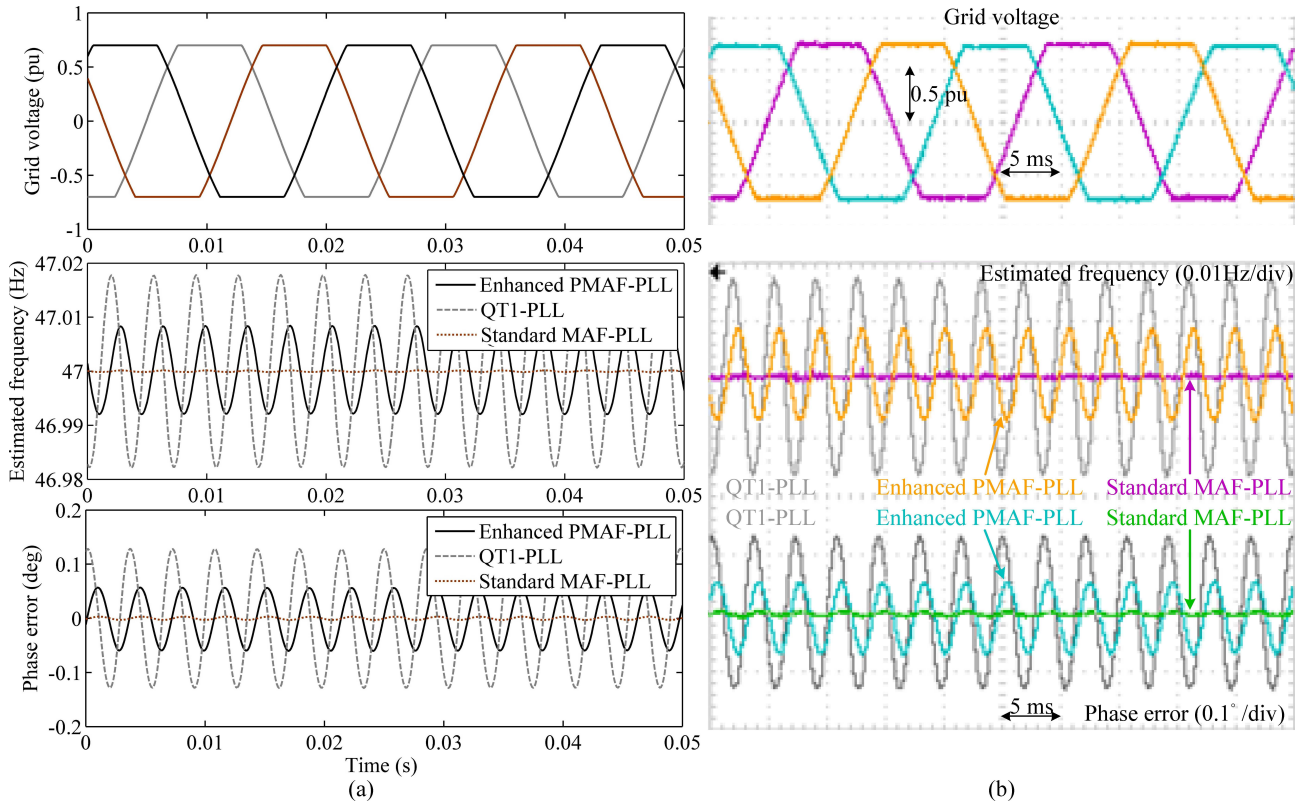

Fig. 13. (a) Simulation and (b) experimental results under the test case 3.

phase angle jumps is achieved. Table I summarizes the control parameters of all PLLs under analysis.

The following three test cases are designed.

1) Test case 1: The grid voltage experiences a phase-angle jump of $+20°$. The grid frequency is at its nominal value during this test.
2) Test case 2: The grid frequency undergoes a -3 Hz step change.
3) Test case 3: All three phases of the grid voltage are clamped at 0.7 pu. The total harmonic distortion of the grid voltage is 13.76%. During this test, the grid frequency is fixed at 47 Hz to take into account the effect of grid frequency variation on the filtering capability of the PLLs.

Figs. 11 and 12 show the simulation and experimental results under the test cases 1 and 2, respectively. It can be observed that the enhanced PMAF-PLL has the fastest dynamic response among all PLLs.

Fig. 13 evaluates the PLLs performance under the test case 3. The standard MAF-PLL, as shown, has the highest filtering capability, and the enhanced PMAF-PLL has the second best performance in this test.

VIII. Conclusion

In this letter, the small-signal modeling of the SRF-PLL with MAF-based prefiltering stage (briefly called, the PMAF-PLL) was presented. This model significantly simplifies the stability analysis and dynamic performance studies. A simple yet effective method to compensate for the phase and amplitude errors of the PMAF-PLL in the presence of frequency drifts was then proposed and its effectiveness was confirmed through a performance comparison with the state-of-the-art PLLs. The equivalence of the PMAF-PLL and SVFT-PLL was also proved, which implies that the small-signal model of the PMAF-PLL and the method presented to enhance its performance are also valid for the SVFT-PLL.

References

[1] S. Golestan, J. M. Guerrero, "Five approaches to deal with problem of DC offset in Phase-Locked Loop algorithms: design considerations and performance evaluations," *IEEE Trans. Power Electron.*, vol. 31, no. 1, pp. 948-661, Jan. 2016.

[2] J. M. Maza-Ortega, J. A. Rosendo-Macias, A. Gomez-Exposito, S. Ceballos-Mannozzi, and M. Barragan-Villarejo, "Reference current computation for active power filters by running DFT techniques," *IEEE Trans. Power Del.*, vol. 25, no. 3, pp. 446-456, Jul. 2010.

[3] M. Liserre, T, Sauter, and J. Y. Hung, "Future energy systems: Integrating renewable energy sources into the smart power grid through industrial electronics," *IEEE Ind. Electron. Mag.*, vol. 4, no. 1, pp. 18-37, Mar. 2010.

[4] S. Golestan, F. D. Freijedo, and J. M. Guerrero, "A systematic approach to design high-order phase-locked loops," *IEEE Trans. Power Electron.*, vol. 30, no. 6, pp. 2885-2890, Jun. 2015.

[5] S. Golestan, M. Ramezani, J. M. Guerrero, F. D. Freijedo, and M. Monfared, "Moving average filter based phase-locked loops: performance analysis and design guidelines," *IEEE Trans. Power Electron.*, vol. 29, no. 6, pp. 2750-2763, Jun. 2014.

[6] M. Karimi-Ghartemani, S. A. Khajehoddin, P. K. Jain, and A. Bakhshai, "Derivation and design of in-loop filters in phase-locked loop systems," *IEEE Trans. Instrum. Meas.*, vol. 61, no. 4, pp. 930-940, Apr. 2012

[7] I. Carugati, S. Maestri, P. G. Donato, D. Carrica, and M. Benedetti, "Variable sampling period filter PLL for distorted three-phase systems," *IEEE Trans. Power Electron.*, vol. 27, no. 1, pp. 321-330, Jan. 2012.

[8] F. G. Espin, E. Figueres, and G. Garcera, "An adaptive synchronous reference-frame phase-locked loop for power quality improvement in a polluted utility grid," *IEEE Trans. Ind. Electron.*, vol. 59, no. 6, pp. 2718-2731, Jun. 2012.

[9] S. Golestan, M. Ramezani, J. M. Guerrero, and M. Monfared, "*dq*-frame cascaded delayed signal cancellation-based PLL: Analysis, design, and comparison with moving average filter-based PLL," *IEEE Trans. Power Electron.*, vol. 30, no. 3, pp. 1618-1632, Mar. 2015.

[10] Y. F. Wang, and Y. Li, "Grid synchronization PLL based on cascaded delayed signal cancellation," *IEEE Trans. Power Electron.*, vol. 26, no. 7, pp. 1987-1997, Jul. 2011.

[11] Y. F. Wang, and Y. W. Li, "Analysis and digital implementation of cascaded delayed-signal-cancellation PLL," *IEEE Trans. Power Electron.*, vol. 26, no. 4, pp. 1067-1080, Apr. 2011.

[12] M. Rashed, C. Klumpner, and G. Asher, "Repetitive and resonant control for a single-phase grid-connected hybrid cascaded multilevel converter," *IEEE Trans. Power Electron.*, vol. 28, no. 5, pp. 2224-2234, May 2013.

[13] X. Guo, W. Wu, and Z. Chen, "Multiple-complex coefficient-filter based phase-locked loop and synchronization technique for three-phase grid-interfaced converters in distributed utility networks," *IEEE Trans. Ind. Electron.*, vol. 58, no. 4, pp. 1194-1204, Apr. 2011.

[14] W. Li, X. Ruan, C. Bao, D. Pan, and X. Wang, "Grid synchronization systems of three-phase grid-connected power converters: a complex-vector-filter perspective," *IEEE Trans. Ind. Electron.*, vol. 61, no. 4, pp. 1855-1870, Apr. 2014.

[15] S. Chandrasekaran and R. Kanagaraj, "Adaptive sampling period adjusted sliding DFT for synchronous reference frame PLL," *in Proc. IEEE International Conf. Power Electronics, Drives and Energy Systems (PEDES)*, 2014, pp. 1-4.

[16] F. A. S. Neves, M. C. Cavalcanti, H. E. P. de Souza, F. Bradaschia, E. J. Bueno, and M. Rizo, "A generalized delayed signal cancellation method for detecting fundamental-frequency positive-sequence three-phase signals," *IEEE Trans. Power Del.*, vol. 25, no. 3, pp. 1816-1825, Jul. 2010.

[17] S. Golestan, F. D. Freijedo, A. Vidal, A. G. Yepes, J. M. Guerrero, and J. Doval-Gandoy, "An efficient implementation of generalized delayed signal cancellation PLL," *IEEE Trans. Power Electron.*, vol. 31, no. 2, pp. 1085-1094, Feb. 2016.

[18] P. Rodriguez, R. Teodorescu, I. Candela, A. V. Timbus, M. Liserre, and F. Blaabjerg, "New positive-sequence voltage detector for grid synchronization of power converters under faulty grid conditions," *in Proc. IEEE 37th Annu. Power Electron. Spec. Conf. (PESC), 2006*, pp. 1-7.

[19] E. Robles, S. Ceballos, J. Pou, J. Martin, J. Zaragoza, and P. Ibanez, "Variable-frequency grid sequence detector based on a quasi-ideal low-pass filter stage and a phase-locked loop," *IEEE Trans. Power Electron.*, vol. 25, no. 10, pp. 2552-2563, Oct. 2010.

[20] E. Robles, S. Ceballos, J. Pou, J. Zaragoza, and I. Gabiola, "Grid synchronization method based on a quasi-ideal low-pass filter stage and a phase-locked loop," *in Proc. IEEE Power Electron. Spec. Conf.*, Rhodes, Greece, Jun., 2008, pp. 4056-4061.

[21] M. Mirhosseini, J. Pou, V. G. Agelidis, E. Robles, and S. Ceballos, "A three-phase frequency-adaptive phase-locked loop for independent single-phase operation," *IEEE Trans. Power Electron.*, vol. 29, no. 12, pp. 6255-6259 , Dec. 2014.

[22] F. A. S. Neves, H. E. P. de Souza, F. Bradaschia, M. C. Cavalcanti, M. Rizo, and F. J. Rodriguez, "A space-vector discrete fourier transform for unbalanced and distorted three-phase signals," *IEEE Trans. Ind. Electron.*, vol. 57, no. 8, pp. 2858-2867, Aug. 2010.

[23] F. A. S. Neves, H. E. P. de Souza, M. C. Cavalcanti, F. Bradaschia, and E. J. Bueno, "Digital filters for fast harmonic sequence component separation of unbalanced and distorted three-phase signals," *IEEE Trans. Ind. Electron.*, vol. 59, no. 10, pp. 3847-3859, Oct. 2012.

[24] F. D. Freijedo, J. Doval-Gandoy, O. Lopez, and E. Acha, "Tuning of phase-locked loops for power converters under distorted utility conditions," *IEEE Trans. Ind. Appl.*, vol. 45, no. 6, pp. 2039-2047, Nov. 2009.

[25] M. Karimi Ghartemini, "Linear and pseudolinear enhanced phased-locked loop (EPLL) structures," *IEEE Trans. Ind. Electron.*, vol. 61, no. 3, pp. 1464-1474, Mar. 2014.

[26] S. Golestan, F. D. Freijedo, A. Vidal, J. M. Guerrero, and J. Doval Gandoy, "A quasi-type-1 phase-locked loop structure," *IEEE Trans. Power Electron.*, vol. 29, no. 12, pp. 6264-6270, Dec. 2014.